V European Conference on Computational Fluid Dynamics
ECCOMAS CFD 2010
J. C. F. Pereira and A. Sequeira (Eds)
Lisbon, Portugal,14-17 June 2010

3D TWO-PHASE FLOW SIMULATIONS WITH THE EXTENDED FINITE ELEMENT METHOD (XFEM)

Henning Sauerland*, Thomas-Peter Fries†

*Chair for Computational Analysis of Technical Systems (CATS),
RWTH Aachen University
Schinkelstrasse 2, 52062 Aachen, Germany
e-mail: sauerland@cats.rwth-aachen.de
†Chair for Computational Analysis of Technical Systems (CATS),
RWTH Aachen University
Schinkelstrasse 2, 52062 Aachen, Germany
e-mail: fries@cats.rwth-aachen.de

Key words: extended finite element method, two-phase flow, surface tension, hexahedral mesh

Abstract. *Based on a validated two-dimensional XFEM code for two-phase flows, this work deals with the extension of this code to three spatial dimensions using structured hexahedral meshes. Surface tension effects are considered, resulting in a discontinuous pressure field. The treatment of hexahedral elements which are cut by the interface is shown. In contrast to linear tetrahedral elements, the discontinuity inside trilinear hexahedral elements is in general not linear but curved. As the XFEM introduces discontinuous functions in the approximation space the hexahedral elements need to be subdivided for integration purposes. Moreover, it is shown how integration points can be placed on the discontinuity itself, which is important for the evaluation of the surface-tension term. Numerical results show the correct prediction of the surface tension and the resulting jump in the pressure field is captured accurately.*

1 INTRODUCTION

Multi-phase flow problems are a challenging field of computational mechanics, as one has to account for the moving interface between the phases. Furthermore, if surface tension effects have to be considered, a discontinuous pressure field exists. Interface-tracking methods generally lack the ability to allow for topology changes and interface-capturing methods often show accuracy problems at least if no mesh refinement is applied near the interface. The XFEM is employed in order to circumvent the disadvantages of standard interface-capturing methods. By applying so called enrichments it is possible to include known solution characteristics, e.g. across the interface, into the approximation space[1, 2, 3]. Thus, the XFEM allows the approximation of discontinuities inside elements with optimal accuracy.

In [4] the XFEM has been successfully applied to two-phase flow problems in 2D. However, three-dimensional numerical simulations are often indispensable for problems of practical relevance. This work deals with the extension of the validated two-dimensional XFEM code to three spatial dimensions using structured hexahedral meshes. The focus is on the special quadrature techniques used, both, in the hexahedra and on the fluid-fluid interface.

The outline is as follows: Section 2 starts with the governing equations of 3D instationary, incompressible, isothermal two-phase flow and the concept of the implicit interface description. In Section 3, the XFEM is introduced. Section 4 gives the resulting weak formulation and in Section 5, the special quadrature procedure in enriched elements is described. Section 6 presents numerical results and a final conclusion is drawn in Section 7.

2 GOVERNING EQUATIONS

We consider a three-dimensional computational domain $\Omega \subset \mathbb{R}^3$ with boundary $\Gamma = \partial\Omega$. The boundary can be decomposed into a Dirichlet and Neumann boundary, Γ_u and Γ_h respectively, forming a complementary subset of the boundary Γ, i.e. $\Gamma_u \cup \Gamma_h = \Gamma$ and $\Gamma_u \cap \Gamma_h = \emptyset$. The normal vector on Γ is denoted by $\boldsymbol{n}$. The domain Ω encloses two immiscible Newtonian fluids in $\Omega_1(t)$ and $\Omega_2(t)$. These two phases are separated by a moving interface $\Gamma_d(t)$, where $\hat{\boldsymbol{n}}$ is the normal vector on Γ_d as shown in Figure 1 for a two-dimensional example.

The fluid velocity $\boldsymbol{u}(\boldsymbol{x}, t)$ and pressure $p(\boldsymbol{x}, t)$ for each phase $j = 1, 2$ are then governed by the instationary, incompressible Navier-Stokes equations in velocity-pressure formulation:

$$\begin{aligned} \rho_j \left(\frac{\partial \boldsymbol{u}}{\partial t} + \boldsymbol{u} \cdot \nabla \boldsymbol{u} - \boldsymbol{f} \right) - \nabla \cdot \boldsymbol{\sigma} &= 0 \quad \text{in } \Omega_j(t) \times [0, T] \\ \nabla \cdot \boldsymbol{u} &= 0 \quad \text{in } \Omega_j(t) \times [0, T] \end{aligned} \tag{1}$$

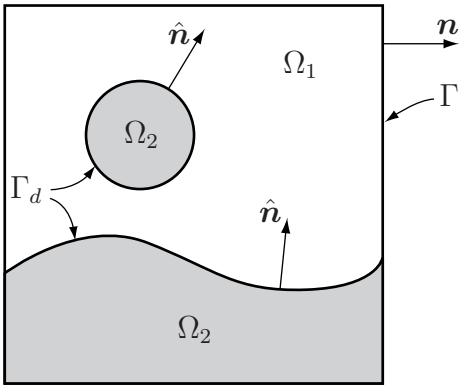

Figure 1: 2D representation of the computational domain.

with ρ_j being the density of the respective fluid. The stress tensor $\boldsymbol{\sigma}$ is defined by

$$\boldsymbol{\sigma}(\boldsymbol{u}, p) = -p\mathbf{I} + 2\eta_j \boldsymbol{\varepsilon}(\boldsymbol{u}) \quad \text{with} \quad \boldsymbol{\varepsilon}(\boldsymbol{u}) = \frac{1}{2}\left(\nabla \boldsymbol{u} + (\nabla \boldsymbol{u})^T\right), \tag{2}$$

μ_j the corresponding dynamic viscosity and $\mathbf{I}$ the identity tensor. The Dirichlet and Neumann boundary conditions Γ are given by

$$\boldsymbol{u} = \hat{\boldsymbol{u}} \quad \text{on } \Gamma_u \times [0, T], \tag{3}$$

$$\boldsymbol{n} \cdot \boldsymbol{\sigma} = \hat{\boldsymbol{h}} \quad \text{on } \Gamma_h \times [0, T] \tag{4}$$

where $\hat{\boldsymbol{u}}$ and $\hat{\boldsymbol{h}}$ are prescribed velocity and stress values. At the interface, typically the following conditions are prescribed

$$[\boldsymbol{u}]_{\Gamma_d} = \mathbf{0} \quad \text{on } \Gamma_d(t) \times [0, T], \tag{5}$$

$$[\hat{\boldsymbol{n}} \cdot \boldsymbol{\sigma}]_{\Gamma_d} = \gamma \kappa \hat{\boldsymbol{n}} \quad \text{on } \Gamma_d(t) \times [0, T]. \tag{6}$$

γ is the surface tension coefficient, κ the curvature of Γ_d and $[f]_{\Gamma_d}$ defines the jump of f across the interface Γ_d. The initial solution is defined by a divergence-free velocity field:

$$\boldsymbol{u}(\boldsymbol{x}, 0) = \hat{\boldsymbol{u}}_0(\boldsymbol{x}) \quad \text{in } \Omega(t = 0). \tag{7}$$

2.1 Description of the interface

In the framework of the XFEM, the level-set method is used to describe the inner-element interface Γ_d. The zero-level of the introduced scalar level-set function ϕ represents the interface. In this work, ϕ has the signed-distance property:

$$\phi(\boldsymbol{x}) = \pm \min_{\boldsymbol{x}^* \in \Gamma_d} \|\boldsymbol{x} - \boldsymbol{x}^*\|, \quad \forall \boldsymbol{x} \in \Omega. \tag{8}$$

If the interface Γ_d is moving throughout the simulation, $\phi(\boldsymbol{x}, t)$ needs to be updated in each step. Therefore, the level-set transport equation

$$\frac{\partial \phi}{\partial t} + \boldsymbol{u}(\boldsymbol{x}, t) \cdot \nabla \phi = 0 \quad \text{in } \Omega \times [0, T] \tag{9}$$

is solved, where $\boldsymbol{u}(\boldsymbol{x}, t)$ is the fluid velocity and

$$\phi(\boldsymbol{x}, 0) = \hat{\phi}_0(\boldsymbol{x}) \quad \text{in } \Omega(t_0 = 0) \tag{10}$$

are the initial level-set values. Eq. (1) and (9) are evaluated in a strongly coupled sense.

3 EXTENDED FINITE ELEMENT METHOD (XFEM)

Due to the density and viscosity differences between the phases in a two-phase flow problem with surface tension a kink in the velocity field and a jump in the pressure field along the interface is encountered. In order to consider these non-polynomial behavior, the approximation space is enriched with these known solution characteristics[1, 2]. The basic concept of the XFEM also holds for three spatial dimensions. In this work only the pressure degrees of freedom are enriched, resulting in the following XFEM approximation:

$$p^h(\boldsymbol{x}) = \underbrace{\sum_{i \in I} N_i(\boldsymbol{x}) p_i}_{\text{strd. FE approx.}} + \underbrace{\sum_{i \in I^*} M_i(\boldsymbol{x}, t) a_i}_{\text{enrichment}} . \tag{11}$$

$N_i(\boldsymbol{x})$ is the standard FE shape function for node i, I is the set of all nodes in the domain, $M_i(\boldsymbol{x}, t)$ are the local enrichment functions, a_i are the additional XFEM unknowns and I^* is the set of enriched nodes. These are the nodes of elements cut by the interface. We are using the shifted definition of the local enrichment function[5]:

$$M_i(\boldsymbol{x}, t) = N_i(\boldsymbol{x}) \cdot [\psi(\boldsymbol{x}, t) - \psi(\boldsymbol{x}_i, t)] \quad \forall i \in I^* \tag{12}$$

with $\psi(\boldsymbol{x}, t)$ being the global enrichment function. For the discontinuous pressure field, the sign-enrichment is chosen here:

$$\psi_{\text{sign}}(\boldsymbol{x}, t) = \text{sign}\left(\phi(\boldsymbol{x}, t)\right) = \begin{cases} -1 & : \ \phi(\boldsymbol{x}, t) < 0, \\ 0 & : \ \phi(\boldsymbol{x}, t) = 0, \\ 1 & : \ \phi(\boldsymbol{x}, t) > 0. \end{cases} \tag{13}$$

The velocity and level-set values are interpolated using the standard FE shape functions:

$$\boldsymbol{u}^h(\boldsymbol{x}) = \sum_{i \in I} N_i(\boldsymbol{x}) \boldsymbol{u}_i, \quad \phi^h(\boldsymbol{x}) = \sum_{i \in I} N_i(\boldsymbol{x}) \phi_i. \tag{14}$$

4 WEAK FORMULATION

The following SUPG/PSPG-stabilized weak formulation results: Find $\boldsymbol{u}^h \in \mathcal{S}_u^h$ and $p^h \in \mathcal{S}_p^h$ such that $\forall \boldsymbol{w}^h \in \mathcal{V}_u^h$, $\forall q^h \in \mathcal{V}_p^h$:

$$\begin{aligned}\int_\Omega \boldsymbol{w}^h \cdot \left[\rho_j \left(\frac{\partial \boldsymbol{u}^h}{\partial t} + \boldsymbol{u}^h \cdot \nabla \boldsymbol{u}^h - \boldsymbol{f}\right) + \nabla p^h + \mu_j \nabla \left(\nabla \boldsymbol{u}^h + \left(\nabla \boldsymbol{u}^h\right)^T\right)\right] \, d\Omega \\ + \int_\Omega q^h \nabla \cdot \boldsymbol{u}^h \, d\Omega + \sum_{e=1}^{n_{\mathrm{el}}} \int_{\Omega_{el}^e} \tau_{\mathrm{s}} \left(\boldsymbol{u}^h \cdot \nabla \boldsymbol{w}^h + \frac{1}{\rho_j} \nabla q^h\right) \\ \cdot \left[\rho_j \left(\frac{\partial \boldsymbol{u}^h}{\partial t} + \boldsymbol{u}^h \cdot \nabla \boldsymbol{u}^h - \boldsymbol{f}\right) + \nabla p^h + \mu_j \nabla \left(\nabla \boldsymbol{u}^h + \left(\nabla \boldsymbol{u}^h\right)^T\right)\right] \, d\Omega \\ = \int_{\Gamma_h} \boldsymbol{w}^h \cdot \hat{\boldsymbol{h}} \, d\Gamma + \int_{\Gamma_d} \gamma \kappa \boldsymbol{w}^h \cdot \hat{\boldsymbol{n}} \, d\Gamma\end{aligned} \tag{15}$$

with n_{el} the number of elements. The pressure and the continuity equation are treated fully implicitly and the force term is assumed to be stationary and constant. The following test and trial function spaces are chosen:

$$\mathcal{S}_u^h = \left\{\boldsymbol{u}^h \,|\, \boldsymbol{u}^h \in (\mathcal{H}^{1h})^3, \boldsymbol{u}^h = \hat{\boldsymbol{u}}^h \text{ on } \Gamma_d\right\}, \tag{16}$$

$$\mathcal{V}_u^h = \left\{\boldsymbol{w}^h \,|\, \boldsymbol{w}^h \in (\mathcal{H}^{1h})^3, \boldsymbol{w}^h = \boldsymbol{0} \text{ on } \Gamma_d\right\}, \tag{17}$$

$$\mathcal{S}_p^h = \mathcal{V}_p^h = \left\{q^h \,|\, q^h \in \mathcal{L}_0^2\right\}, \tag{18}$$

with $\mathcal{H}^{1h} \subseteq \mathcal{H}^1$ a finite dimensional Sobolev space. The stabilization parameter τ_{s} is chosen according to [6]:

$$\tau_{\mathrm{s}} = \left(\left(\frac{2}{\Delta t}\right)^2 + \left(\frac{2|\boldsymbol{u}^h|_2}{h_e}\right)^2 + \left(\frac{4\nu}{h_e^2}\right)^2\right)^{-\frac{1}{2}} \tag{19}$$

with $\nu = \mu/\rho$ the kinematic viscosity and h_e the element length. In elements cut by the interface, the parameters μ and ρ are averaged.

The weak formulation of the level-set transport equation follows to: Find $\phi^h \in \mathcal{S}_\phi^h$ such that $\forall \boldsymbol{w}^h \in \mathcal{V}_\phi^h$:

$$\begin{aligned}\int_\Omega \boldsymbol{w}^h \cdot \left(\frac{\partial \phi^h}{\partial t} + \boldsymbol{u}^h \cdot \nabla \phi^h\right) \, d\Omega \\ + \sum_{e=1}^{n_{\mathrm{el}}} \int_{\Omega_{el}^e} \tau_{\mathrm{s}} \left(\boldsymbol{u}^h \cdot \nabla \boldsymbol{w}^h\right) \cdot \left(\frac{\partial \phi^h}{\partial t} + \boldsymbol{u}^h \cdot \nabla \phi^h\right) \, d\Omega = \ 0.\end{aligned} \tag{20}$$

The temporal discretization is evaluated by means of the Crank-Nicolson method. It is noted that special care is needed for the XFEM in combination with time-stepping, see [7].

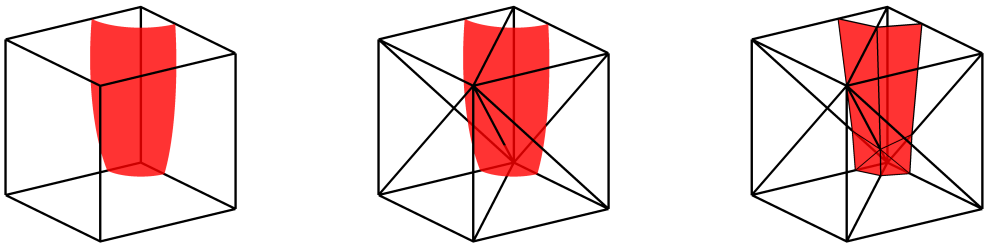

Figure 2: Linearization of the curved interface in a reference element by decomposition of the hexahedron into linear tetrahedral elements.

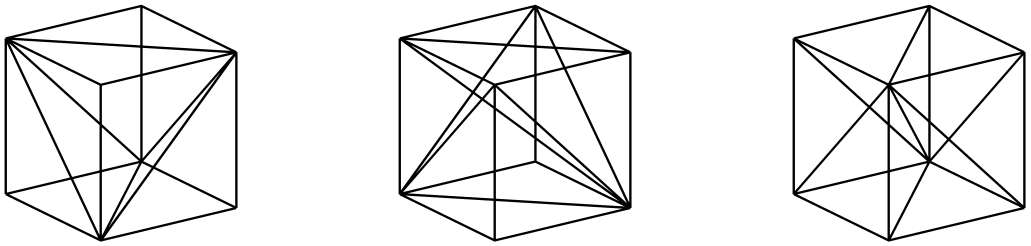

(a) 5 tetrahedra. (b) 6 tetrahedra. (c) 6 tetrahedra.

Figure 3: Possible decompositions of a hexahedron into tetrahedra.

5 NUMERICAL INTEGRATION IN 3D

In the context of the XFEM in 3D, the same difficulties regarding the quadrature of the weak form appear as in 2D. Due to the inclusion of the discontinuous enrichment functions in the approximation space (cf. eq. (13)), the resulting shape functions in cut elements also comprise jumps across the interface. Standard Gauss quadrature requires smoothness of the integrands. Hence, in enriched elements the application of the Gauss quadrature is not reasonable as the accuracy decreases significantly. Therefore, elements including discontinuous shape functions require special treatment of the quadrature of the weak form.

5.1 Element decomposition

It is common in the XFEM to partition cut elements into sub-elements which align with the interface for integration purposes, see e.g. [1, 2, 3]. One has to note that (according to quadrilateral elements in 2D) the interface inside trilinear hexahedral elements is in general not linear but curved, in contrast to linear tetrahedra. This fact complicates the exact partitioning into sub-elements that align with the discontinuity. In order to eliminate the problem of the curved interface, the hexahedra are decomposed into tetrahedra where linear interpolation functions are employed. The resulting "linearized" zero-level of the level-set function is piecewise planar (cf. Fig. 2). The decomposition of a hexahedron into tetrahedra is not unique, see Fig. 3 for different alternatives where 5 or 6

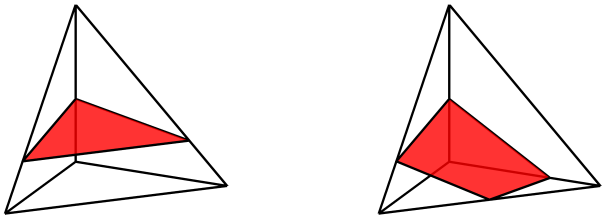

Figure 4: Cutting planes of tetrahedra.

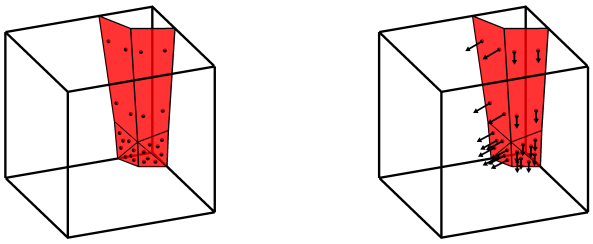

Figure 5: Integration points and normal vectors on the interface in a reference element.

tetrahedra result. In this work, we will use a decomposition into 6 tetrahedra, such that opposite element faces coincide in the orientation of their diagonals resulting from the decomposition (cf. Fig. 3(c)). Thereby, it is ensured that the linearized interfaces in neighbouring, cut elements match at their common element face. After this decomposition each tetrahedron—with a planar interface—can be further subdivided into elements aligned with the interface. The interface in a cut tetrahedral element can either be of triangular or quadrilateral shape in 3D, which leads to a subdivision with (i) a tetrahedron and a pentahedron or (ii) two pentahedra, see Fig. 4. Standard Gauss rules can finally be applied in these tetrahedral and pentahedral elements. The resulting coordinates and weights of the integration points are projected into the real geometry and can be used for the quadrature of the weak formulation. One has to note that the "linearized" interface in the hexahedra is only linear in the reference elements. After the projection into the real element the interface is again curved in general.

5.2 Integration along the interface

The evaluation of the surface tension term in equation (15) requires the quadrature of an integral along the interface. We therefore need to place Gauss points on the interface itself. First of all, the surface tension term is reformulated by means of the Laplace-Beltrami operator[8]. For the closed interfaces considered in this work this leads to:

$$\int_{\Gamma_d} \gamma\kappa\boldsymbol{w}^h \cdot \hat{\boldsymbol{n}}\, d\Gamma = -\int_{\Gamma_d} \gamma\underline{\nabla}\mathrm{id} \cdot \underline{\nabla}\boldsymbol{w}^h\, d\Gamma, \tag{21}$$

where $\underline{\nabla} f = \nabla f - (\nabla f \cdot \hat{\boldsymbol{n}})\hat{\boldsymbol{n}}$ and id is an identity mapping on the interface Γ. The advantage of the reformulation (21) is that the curvature κ of the interface is not needed. In order to evaluate the integral, Gauss points need to be placed on the discontinuity and the normal vectors of the interface elements have to be determined. The intersections of the interface with the element boundaries are calculated using linear interpolation and the level-set values at the element nodes. Gauss points can then be placed on the resulting 2D interface elements and be projected in the according cut tetrahedral element. The normal vectors of the interface elements are easily calculated in the reference domain as the cross-product of two tangential vectors on the interface elements, perpendicular to each other (cf. Fig. 5). Projection to the real element leads to the desired quantities for the evaluation of eq. (21).

6 NUMERICAL RESULTS

6.1 Static bubble

We consider a cubic domain of size $4 \times 4 \times 4\,m$ with a sphere of radius $r = 1\,m$ in the center (cf. Fig. 6(a)). A uniform hexahedral mesh with $30 \times 30 \times 30$ elements is used. The surface tension coefficient is given by $\gamma = 1.0$. Density and viscosity are the same in both phases, $\rho_1 = \rho_2 = 1.0\,kg/m^3$ and $\mu_1 = \mu_2 = 1.0\,kg/s/m$ and no gravitational forces are considered. Hereby, index 2 is the bubble phase and index 1 denotes the surrounding fluid. Then the exact solution of the velocity field is $\boldsymbol{u}(\boldsymbol{x}) = \boldsymbol{0}$ and the pressure is

$$p(\boldsymbol{x}) = \begin{cases} 0, & \forall \boldsymbol{x} \in \Omega_1 \\ \gamma \cdot \kappa, & \forall \boldsymbol{x} \in \Omega_2 \end{cases}. \tag{22}$$

The curvature κ is given by the sum of two curvatures $\kappa = \kappa_1 + \kappa_2 = 1/r_1 + 1/r_2$, with r_1 and r_2 the principal radii of curvature of the surface in 3D[9]. In case of the sphere,

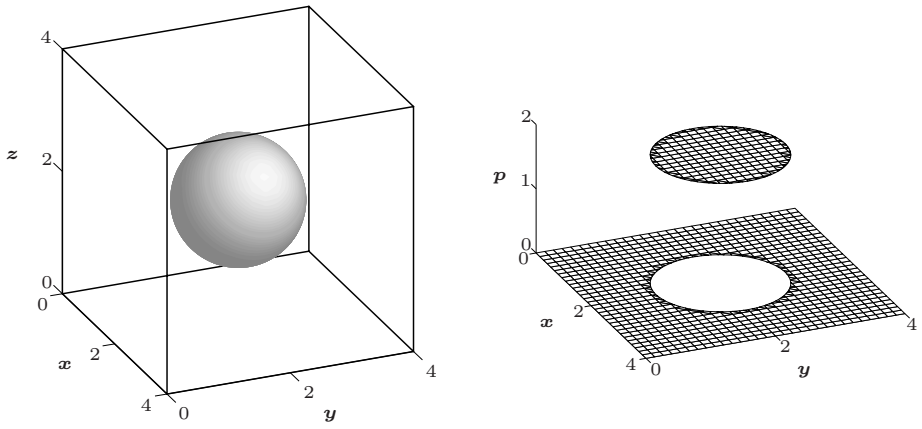

(a) Computational domain. (b) Pressure solution in $z = 2$ slice.

Figure 6: Static bubble test case.

κ is constant and $r_1 = r_2 = r$. Fig. 6(b) shows the pressure solution on a $x - y$ plane through the center of the sphere. As can be seen, the XFEM is able to reproduce the exact pressure difference $\Delta p = 2\,N/m^2$ and the discontinuity across the interface nicely.

6.2 Rising bubble

A rising bubble in a rectangular domain is considered. The dimensions and fluid properties are chosen according to the 2D test case in [4]. The initial diameter of the spherical bubble is set to $d = 0.1\ m$ and the measurement of the computational domain is $2d \times 2d \times 4d$ (x-, y- and z-direction). The fluid properties are $\rho_1 = 1000\,kg/m^3$,

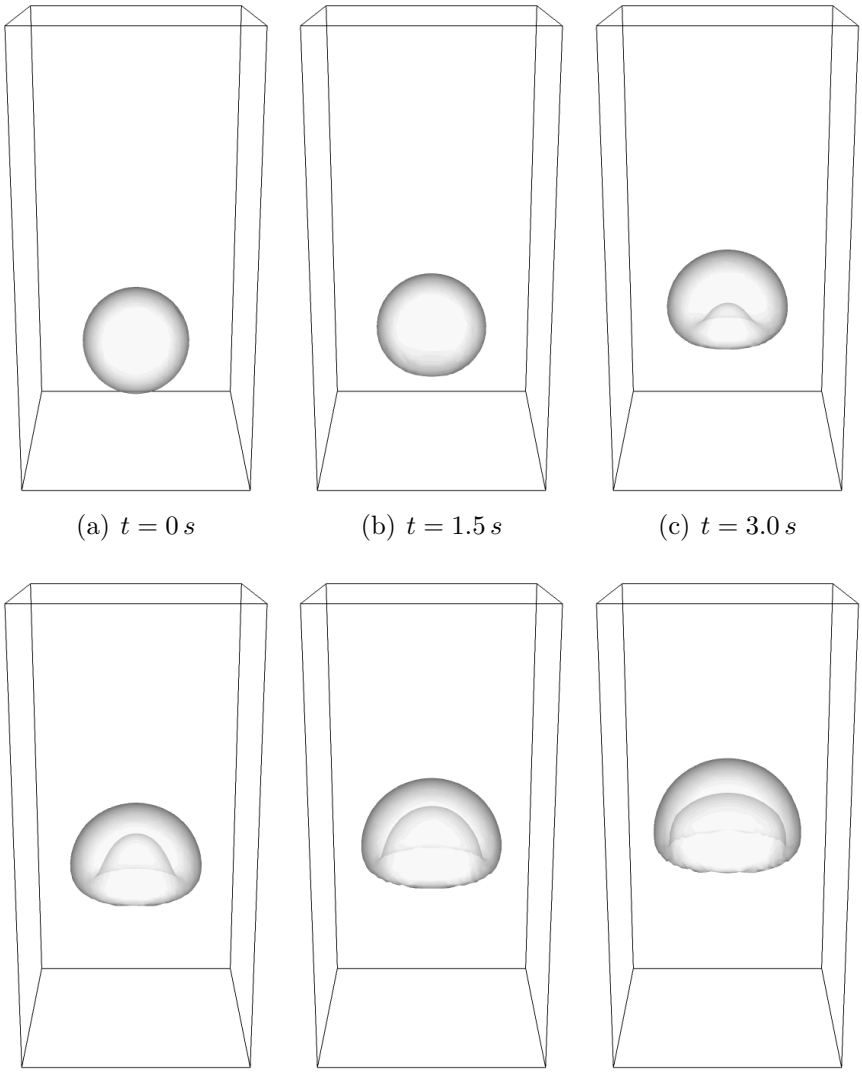

(a) $t = 0\,s$ (b) $t = 1.5\,s$ (c) $t = 3.0\,s$

(d) $t = 4.5\,s$ (e) $t = 6.0\,s$ (f) $t = 7.5\,s$

Figure 7: Rising bubble test case.

$\rho_2 = 1\,kg/m^3$, $\mu_1 = 0.01\,kg/s/m$, $\mu_2 = 0.0001\,kg/s/m$ and the surface tension coefficient $\gamma = 0.001\,kg/s^2$. Index 2 is the bubble phase and index 1 denotes the surrounding fluid. The gravitational forces are set to $f_z = -g = -0.01\,m/s^2$. The Morton number is

$$Mo = \frac{g \cdot \mu_1^4 \cdot (\rho_1 - \rho_2)}{\rho_1^2 \cdot \gamma^3} = 0.01 \tag{23}$$

and the Eötvös number

$$Eo = \frac{g \cdot (\rho_1 - \rho_2) \cdot d^2}{\gamma} = 100. \tag{24}$$

Slip boundary conditions are assumed along all boundaries and the pressure $p = 0\,N/m^2$ is set at the upper boundary. The time step is chosen to $\Delta t = 0.1\,s$ and the spatial resolution using a hexahedral mesh is $30 \times 30 \times 60$ elements. Fig. 7 shows the bubble shape at different time steps.

7 CONCLUSION

The validated 2D two-phase flow XFEM code was successfully extended to the 3D case using hexahedral meshes. Applying the presented quadrature technique, the "exact integration" property of the Gauss quadrature can be maintained also for elements with discontinuous shape functions. Furthermore, it was shown how integration points can be placed on the phase interface in order to evaluate the surface tension term. A stationary bubble test case showed the correct evaluation of the surface tension and the exact reproduction of the discontinuity across the interface. The success of the method is shown by means of a rising bubble simulation.

REFERENCES

[1] T. Belytschko and T. Black, Elastic crack growth in finite elements with minimal remeshing, *Int. J. Num. Meth. Engng.*, **45**, 601–620 (1999).

[2] N. Moës and J. Dolbow and T. Belytschko, A finite element method for crack growth without remeshing, *Int. J. Num. Meth. Engng.*, **46**, 131–150 (1999).

[3] T.P. Fries and T. Belytschko, The generalized/extended finite element method: An overview of the method and its applications, *Int. J. Num. Meth. Engng.*, submitted.

[4] T.P. Fries, The intrinsic XFEM for two-fluid flows, *Int. J. Numer. Methods Fluids*, **60**, 437–471 (2009).

[5] T. Belytschko and N. Moës and S. Usui and C. Parimi, Arbitrary discontinuities in finite elements, *Int. J. Num. Meth. Engng.*, **45**, 993 – 1013 (2001).

[6] F. Shakib and T.J.R. Hughes and Z. Johan, A new finite element formulation for computational fluid dynamics: X. The compressible Euler and Navier-Stokes equations, *Comp. Methods Appl. Mech. Engrg.*, **89**, 141–219 (1991).

[7] T.P. Fries and A. Zilian, On time integration in the XFEM, *Int. J. Numer. Methods Fluids*, **79**, 69–93 (2009)

[8] S. Hysing, A new implicit surface tension implementation for interfacial flows, *Int. J. Numer. Methods Fluids*, **51**, 659–672 (2005).

[9] J.U. Brackbill and D.B. Kothe and C. Zemach, A continuum method for modeling surface tension, *J. Comput. Phys.*, **100**, 335 – 354 (1992).